*Korean J. Chem. Eng.*, 33(7), 2160-2168 (2016)
DOI: 10.1007/s11814-016-0081-y

pISSN: 0256-1115
eISSN: 1975-7220

# Vacuum enhanced membrane distillation for trace contaminant removal of heavy metals from water by electrospun PVDF/$TiO_2$ hybrid membranes

**Rasoul Moradi*, Saeed Mahruz Monfared**, Younes Amini***, and Abolfazl Dastbaz*,†**

*Department of Chemical Engineering, University of Tehran, Tehran, Iran
**Department of Chemical and Petroleum Engineering, Sharif University of Technology, Tehran, Iran
***Department of Chemical Engineering, Isfahan University of Technology, Isfahan, Iran
(*Received 26 August 2015 • accepted 18 March 2016*)

**Abstract**−Electrospun hybrid membranes were synthesized using electrospinning of Poly (vinylidenefluoride) - titanium tetraisopropoxide (PVDF-TTIP) sol. Asymmetric post-treatment of membrane conducted for deprotonation of titanate and making hydrophilic/hydrophobic dual characteristics. The membranes were characterized by various methods such as wettability, scanning electron microscopy, infrared spectroscopy, X-ray diffraction and liquid entry pressure tests. For evaluating the separation performance, these membranes were applied in the VMD process to treat water heavy metal contaminants. The effects of operating parameters such as flow rate, temperature and membrane properties as porosity, on contaminant removal and producing ultra-pure water have been studied.

Keywords: Vacuum Membrane Distillation, PVDF/$TiO_2$, Hydrophobic Membrane, Permeability Measurement, Electrospinning, Metal Removal

## INTRODUCTION

Membrane distillation (MD) is considered as the emerging non-isothermal separation process in which only the vapor molecules of the volatile components could transport through the hydrophobic pores of the membrane [1-3]. This technique is based on the partial vapor pressure difference of the components that performed by thermal gradient across the membrane [4].

Chemical precipitation, adsorption, electrochemical removal and pressure driven processes such as micro and nanofiltration are the traditional techniques for heavy metal contaminant removal from water. These techniques have some disadvantages such as high-energy consumption and incomplete removal. Although reverse osmosis and nanofiltration process are so efficient, but in the low concentration of metal ions (<100 ppm), these techniques could not remove the contaminant completely, especially when the production of ultrapure water is purposed. Complete rejection of non-volatile solutes is potentially distinctive advantages of MD that makes it more interesting topic in some particular areas like water contaminant removal [5]. Regarding various advantages of MD as lower operating temperature and pressure, it is not applicable yet in industrial processes due to its relatively lower product flux in compassion with other well-established water treatment techniques such as nanofiltration and reverse osmosis. Therefore, MD may be implemented as a secondary step after the nanofiltration and reverse osmosis processes to remove heavy metals and reduce potential water contamination. Heavy metals and radionuclides such as uranium have proved to be efficiently removed from the impaired water as reported by Yarlagadda et al. [6]. Recently, MD applied by several researchers for treating of wastewater from wastewater [7]. Nevertheless, MD investigation mostly at the laboratory stage, for example, the research on desalination, ground water treatment, removing volatile organic components and solar heat utilization, is increased dramatically in the following years [8-11]. A large number of studies in this field mainly focus on improving the MD membrane properties. High permeability and hydrophobicity, Low thermal conductivity and good mechanical properties are some of the main characteristics of a good MD membrane. These properties depend on the membrane preparation materials and methods. Organic-inorganic non-woven films are the new class of developed membranes to improve structural and operational properties of them in separation processes. Inorganic materials addition into the polymeric membrane matrix in the forms of nanoparticles, continuum bed or web-like structure, in many cases, improves the physical properties of the membrane. Mechanical strengths of polymeric nanofiber membranes significantly increase with impregnating of inorganic metal oxides such as $Al_2O_3$, $SiO_2$, and $TiO_2$ into their physical structure. Silica-based porous mats have motivated numerous researchers due to their unique characteristics like as highly controllable surface properties and good mechanical strength [12,13]. So, electrospinning is a versatile and simple method for the preparation of such materials by which the synthesizing of the nanometric fibers of both polymeric and composite materials could be done [14-17]. Electrospun fibers that contain functional groups which can form chelates were used in the removing of heavy metals [13]. Furthermore, the fiber mats of organic-inorganic composite materials were successfully synthesized and used for this purpose [18-20].

From the various inorganic materials that have been employed in the preparation of hybrid membranes, as mentioned earlier, Tita-

†To whom correspondence should be addressed.
E-mail: a.dastbaz@ut.ac.ir
Copyright by The Korean Institute of Chemical Engineers.

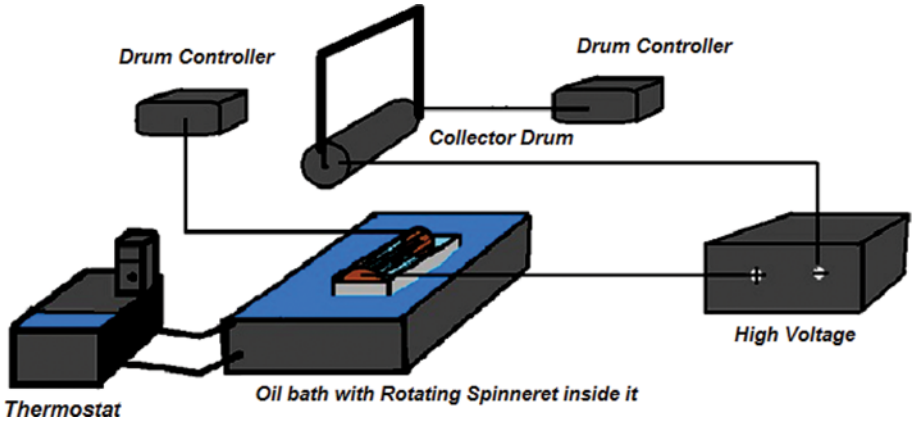


**Fig. 1. Schematic of needle-less electrospinning setup used for producing nanofiber membranes.**

nia ($TiO_2$), regarding its inertness and well-known characteristics, is much more applicable and convenient to use [20].

A most convenient method to synthesize of polymer/Titania hybrid materials is mixing an organic polymer (such as PVDF, etc.) with Titania-alkoxides, such as tetraisopropylorthotitanate (TTIP) followed by hydrolysis and poly-condensation, the so-called sol-gel process [21]. This technique is very compatible for the preparation of polymer/metal oxide hybrid fibrous membranes in combination with an electrospinning technique [22].

One of the objectives of this work was to prepare nanofibrous PVDF/Titania hybrid membrane by electrospinning the organic-inorganic blend solution following by thermal treatment for the sol-gel process of the TTIP. Here were used different rates of thermal processing of the membrane surfaces to introduce double-state wettability properties in the different sides of the membranes. This asymmetric post-treatment was used for producing much more effective MD membranes with higher permeate flux as well as higher separation efficiency. Considering the importance of developing energy and cost-effective methods for water treatment and trace contaminant removal, electrospun non-woven membranes with exclusive properties are very promising in MD applications.

In this work, the possibility of MD implementation in heavy metal trace removal from water using a modified PVDF/$TiO_2$ electrospun membrane was reported. In addition, the needleless electrospinning method with high productivity was applied for preparation of electrospun hybrid membranes. The structure of the prepared nanofibrous hybrid membranes was studied by contact angle (CA), X-ray diffraction (XRD), scanning electron microscopy (SEM), Fourier transform infrared spectroscopy (FTIR) and nitrogen adsorption-desorption tests. Furthermore, the synthesized pristine and modified PVDF nanofibrous membranes were employed in the MD process for the eliminating of trace concentrations of heavy metals from water. The MD separation efficiency for PVDF/$TiO_2$ hybrid membranes was investigated in comparison with PVDF membranes.

## EXPERIMENTAL

### 1. Materials

Poly (vinylidene fluoride) (PVDF), titanium tetra isopropoxide (TTIP or $Ti(OiPr)_4$) and N, N-dimethylformamide (DMF) were purchased from Sigma-Aldrich Co, USA. Metal solutions were prepared from relevant salts of Co (II), Zn (II), Cu (II), Ni (II), Cd (II) and Pb (II) that all were from Merck, Germany. All other reagents and solvents were commercially available.

### 2. Nanofibrous Hybrid Membrane Preparation

A polymer dope solution was prepared by dissolving an appropriate amount of PVDF in the DMF/acetone (50/50) mix solvent to produce 10 wt% of the polymer solution. The TTIP was added into the polymer solution in different concentrations of 0, 5, 10, and 20 wt% (based on polymer weight). Blend solution was stirred vigorously for 3 h at 30 °C and then ultrasound up to 1 h to be homogenized before electrospinning. PVDF/TTIP solutions were used for electrospinning as prepared; this is due to solvent evaporation in solutions by time, which changes polymer solution properties [21].

The homemade electrospinning setup was utilized in this work. As shown in Fig. 1, needleless electrospinning setup consisted of a rotating spinneret in spite of the needle in conventional systems. This system was used for its high productivity in fiber synthesizing. Other parts of this setup included a high voltage power supply that could generate positive DC voltages up to 50 kV, drum controller, and fiber collector. The rotating spinneret was immersed into the thermostat bath for temperature controlling, and its slowly rotating rate was precisely controlled.

Spinneret rotating inside the precursor polymer solution produces tiny droplets that when they reach up to the spinneret in front of the fiber collector are trapped in the high voltage electrical field and electrospun upward to the fiber collector surface. The surface of the collector drum was covered with thin aluminum foil for easy collecting of the fibers and separating the formed membrane sheet without further departure from it. Electrospun PVDF/TTIP films were prepared with a different weight ratio of TTIP in polymer precursor solutions and for solvent evaporation kept overnight in an oven at 35 °C.

### 3. Post-treatment of Membrane

The electrospun membrane films were asymmetric post-treated for inducing the hydrophilic-hydrophobic nature in their both sides. Post-treatment was performed by hydroxylation and deprotonation reactions of TTIP. Dehydroxylation of the membrane surface

for enhancing hydrophobicity was done by heat treatment in oxidation environment. Effects of thermal treatment on PVDF/$TiO_2$ composite membrane have been studied in previous studies [23,24].

**4. Contact Angle Measurement**

Wettability tests of the synthesized membranes were conducted by water contact angle measuring using the sessile drop method by a goniometer (Data-Physics, OCA 20, Germany). Both sides of the membranes were investigated for determining whether the post-treatment changed the hydrophobicity of the membrane surface. To reduce the error, multiple measurements were taken and averaged. The value of contact angle was averaged over at least six repetitions for each membrane/temperature combination. The standard deviation for the all measured contact angles was lower than 4°.

**5. Liquid Entry Pressure (LEP) Measurement**

To measure the LEP of a given membrane, pressure is gradually increased on the feed side of the membrane. The LEP is the pressure at which the first drop of the feed solution appears on the permeate side. The LEP measurement guidelines have been described by Smolders and Franken [24] in detail and have been used by various researchers for both flat-sheet and hollow-fiber membranes [25,26]. Other authors used conductivity changes on the permeate side in a membrane distillation set-up to determine the LEP [27]. In this work, a custom-built device for LEP measurement depicted in Fig. 2 was used to measure the LEP at a controlled temperature.

The gravimetric method was used to assess the prepared electrospun membranes porosity. We used isopentane as the wetting liquid, due to the hydrophobicity of PVDF membranes. The weight of wetting liquid contained in the membrane pores is related to porosity ($\varepsilon$) by Eq. (1).

$$\varepsilon = \frac{(w_1 - w_2)/D_1}{(w_1 - w_2)/D_1 + w_2/D_p} \quad (1)$$

where $w_1$ is the weight of the wet membrane, $w_2$ is the weight of the dry membrane, $D_1$ is the isopentane density and $D_p$ is the polymer density.

**6. Scanning Electron Microscopy (SEM) and Atomic Force Micrograph (AFM)**

A field emission-scanning electronic microscope (FE-SEM, Hitachi, Japan) and Atomic Force Micrograph (ARA-AFM, IRAN) observed the morphology of electrospun nanofibrous membranes. Prior to SEM observation, all of the samples were coated with gold. The average diameter of nanofibers was determined by analyzing the SEM images with an image analyzing software (Image-Pro Plus, Media Cybernetics Inc.).

**7. Spectroscopic Analyses**

Structural studies of the resulting films were carried out using Fourier-transform infrared spectroscopy (FT-IR) of nanofibers with KBr on a spectroscopy instrument (Bruker Tensor 27, USA). X-

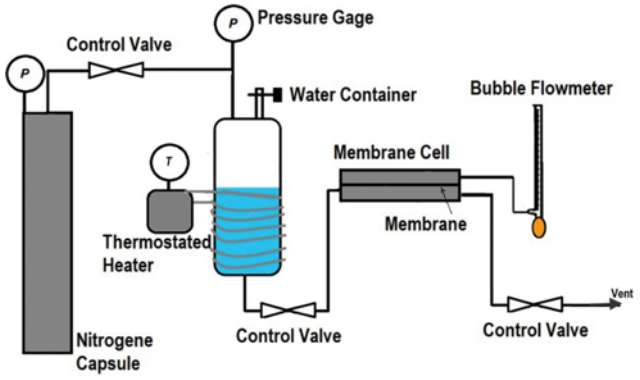


**Fig. 2. Schematic representation of liquid entry pressure (LEP) measurement setup. Water container is equipped with the heater to carry out the LEP experiments in different water temperatures.**

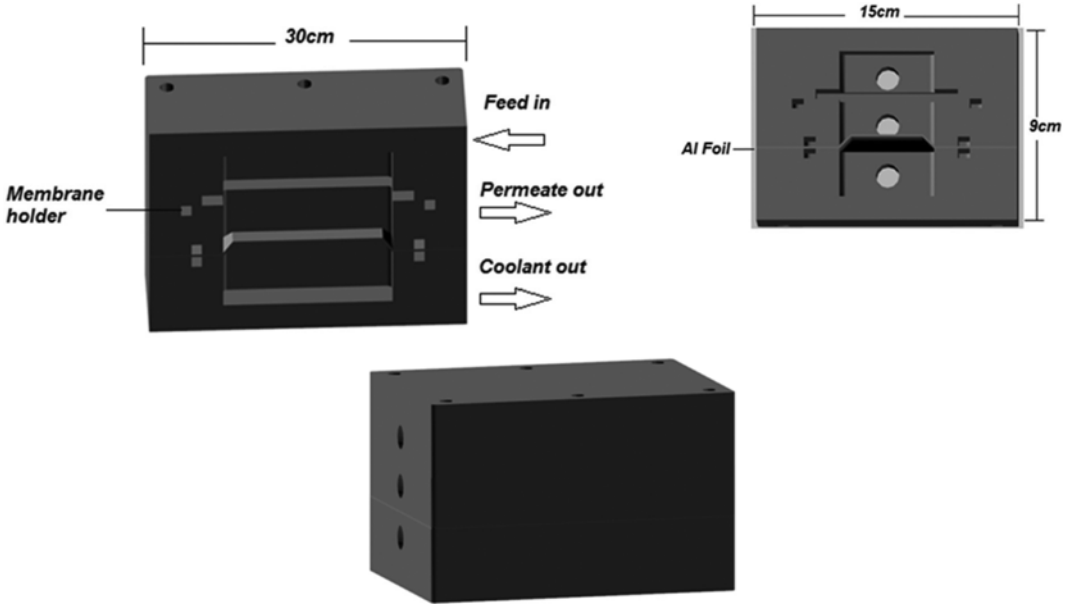


**Fig. 3. Schematic of the employed VMD cell is shown. Cross sectional image of the designed module with dimensions and components are identified.**

ray diffraction (XRD), experiments for crystallographic studies has performed using X-ray diffraction (XRD) instrumentation (Intel, EQuinox 3000, France).

**8. VMD Module Design**

New laboratory-scale MD membrane module was machined from Teflon with outlet and inlet PVC (polyvinyl chloride) tubes of 3/8 inches in inner diameters. The designed module is schematically shown in Fig. 3. This design allows for the turbulence transition of feed steam at the module entrance, which causes to decrease in polarization effects and boundary layer thickness. The square channel in the module is 3×9 cm, so flat sheet membranes require a support in VMD applications. The support was made from sintered stainless steel material. The membrane was sandwiched between two half-cells above the support and the module was completely sealed and held together with several clamps. The total membrane area in this module was about 15 $cm^2$.

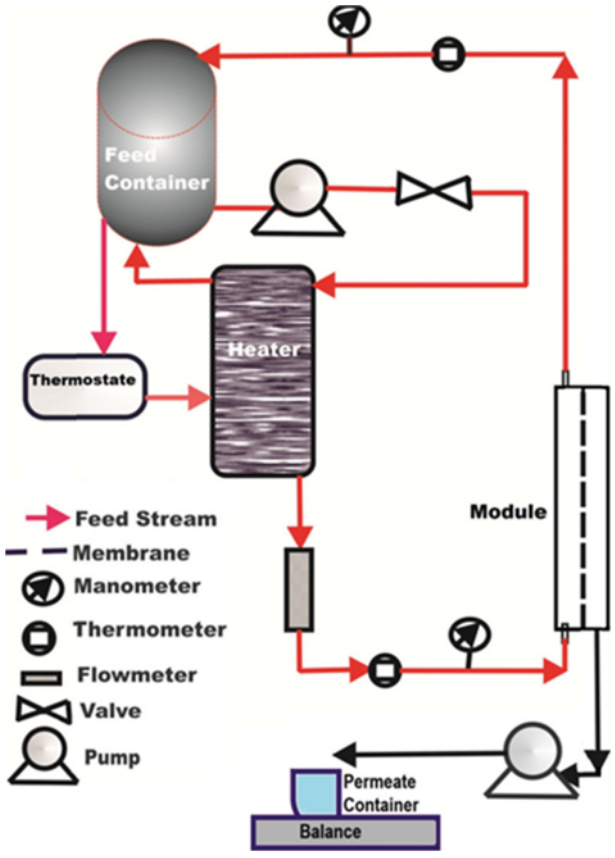


**Fig. 4. Vacuum enhanced membrane distillation flow diagram.**

**9. VMD Experiments**

A schematic of thte experimental VMD trace contaminant removal setup is depicted in Fig. 4. For visibly detecting of the permeate condensation and/or membrane leak from the feed side a sight glass was installed in the permeate line beside the membrane module. For each heavy metal trace removal experiment, a new membrane sample was loaded into the membrane module. The feed solutions contain different trace concentrations of heavy metals were heated in a thermostatic bath up to a definite temperature before entering the module. The total feed solution volume was about 5 L and the solution temperature in the container and the entrance of the module was measured with the J-type thermocouples-digital thermometer with an accuracy of ±1 °C. Hot feed was brought into contact with the membrane by a peristaltic pump, sent due to the applied vacuum in another side of the membrane that water molecules vaporized in the entrance of the membrane pores and diffused to the permeate side. The feed flow rate was set manually by the pumping rate and was measured with a rotameter with an accuracy of ±5% of reading. To prevent saturation and condensation of water in the vacuum side of the module, nitrogen dry gas was blown through it during the heating period. Once the feed temperature attained a steady state, nitrogen stream was turned off and the vacuum was started and one cold trap was employed for collecting permeates during the experiments. The applied vacuum by the vacuum pump was fixed in the range of 2,500±500 Pa and measured by a pressure gage within ±150 Pa accuracy. All parameters were continually monitored during the experiments to ensure that its process had attained steady state.

## RESULTS AND DISCUSSION

**1. Electrospun Membrane Synthesis and Treatment**

Nanofibrous inorganic-organic hybrid membranes, owing to their fascinating characteristics such as high porosity, high permeability, and durability, gather a great amount of interest in membrane sciences. In the present study, these kinds of membranes were prepared by electrospinning of PVDF-TTIP blend solution in different weight ratios of 0, 5, 10, and 20 wt%.

SEM micrographs of synthesized nanofibrous membranes are represented in Fig. 5. As shown, by increasing the concentration of

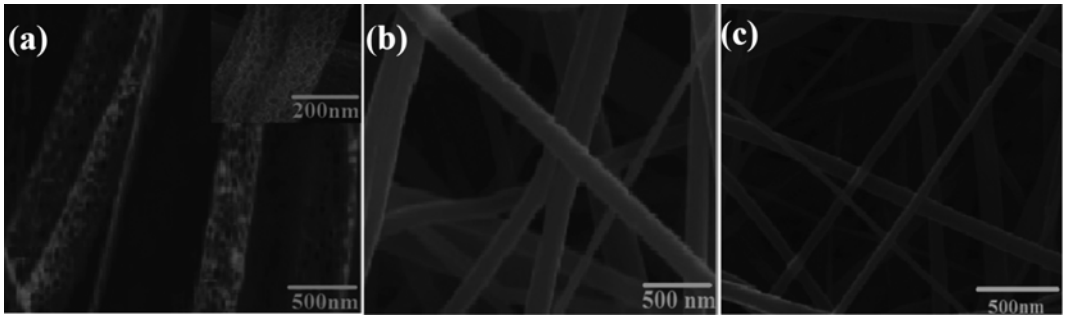


**Fig. 5. SEM images of prepared membrane (a) pristine membrane (b) 5% TTIP content (c) 20% TTIP content.**

**Table 1. Comparative analyses results for various prepared membranes**

| Membrane | TTIP conc. (wt%) | LEP (kPa) | CA (°) | Porosity (%) | Mean pore size (nm) | Young modulus (MPa) |
|---|---|---|---|---|---|---|
| M1 | 0 | 75±4 | 124±2 | 73±3 | 300±15 | 400±50 |
| M2 | 5 | 110±5 | 125±2 | 72±3 | 325±10 | 450±70 |
| M3 | 10 | 125±5 | 130±3 | 74±3 | 320±10 | 490±50 |
| M4 | 20 | 140±4 | 135±3 | 75±3 | 270±15 | 550±40 |
| M′3 (treated) | 10 | 155±5 | 145±5 | 72±3 | 320±10 | 510±40 |

TTIP in the precursor polymer solution, the average diameter of synthesized nanofibers reduced. This is due to reducing of the polymer solution viscosity with the addition of low molecular weight inorganic as TTIP [27]. The average diameters of the synthesized nanofibers with increasing the TTIP weight ratios from 0 to 20 wt%, change from 400±50 nm to 250±40 nm.

The solution viscosity decreasing with the addition of TTIP strongly affects the electrospinning process at the same spinning flow rate and applying voltage cause of the formation of the thinner and smaller tailored cone at the needle tip. This has resulted in thinner nanofibers and in many cases fragile structures of the produced membrane, then the appropriate amount of TTIP must be added into the polymer matrix. Table 1 represents the change in different properties of the synthesized PVDF with weight ratios of added TTIP. In addition, the properties of thermally treated membranes are tabulated. In spite of enhancement in the porosity of the hybrid membranes, some other properties as mechanical strength and hydrophobicity of the PVDF/TTIP nanofibrous membranes do not increase with the addition of TTIP inorganic materials. Thermal treatment is the main post-treatment method for improving these properties.

As can be seen, thermal treatment of PVDF/TTIP affects the mechanical strength, thermal stability, and hydrophobicity of the synthesized membranes. Although the addition of TTIP to PVDF membrane enhanced its morphology and porosity, but the mechanical stability of these hybrid membranes was not markedly improved. But, post thermal treatment increases the average diameters of the PVDF/TTIP nanofibers. The main drawback of the thermal treatment process is decreasing of the membrane permeability due to calcinations of nanofibers imprinted Ti-OH groups and producing Ti-O-Ti bonds. This process causes shrinkage in the membrane pores and pore size decreasing. For investigating this process, FT-IR analysis was carried out and spectra for pristine, hybrid and post-treated PVDF nanofibrous membranes are shown in Fig. 6. As shown, for non-treated membrane three sharp peaks centered at 880 (C-F bond), 1,180 (C-C bond), 1,400 $cm^{-1}$ (C-F bond), 475 $cm^{-1}$ (Ti-O-Ti) and 3,200 $cm^{-1}$ (for Ti-OH bond), where for the post-treated nanofibers the intensity of Ti-O peak strongly increases regarding dehydroxylation and calcination process that produce the web structure of Ti-O-Ti bonds [28].

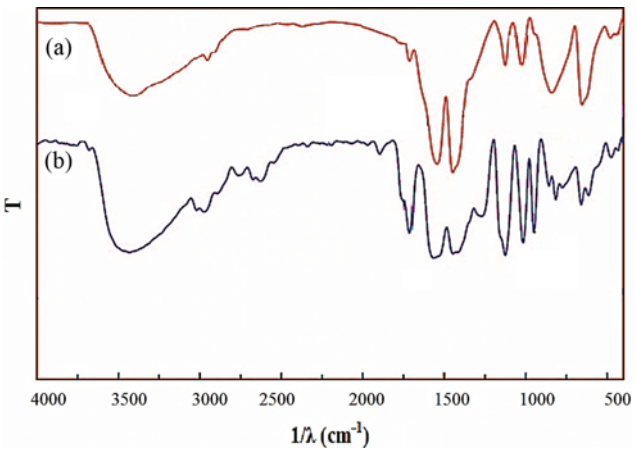


**Fig. 6. FT-IR spectrum of (a) PVDF/TTIP membrane (M3) (b) thermal treated PVDF/TTIP membrane (M′3).**

In the result of hydroxyl group elimination from the nanofibers surface, the wettability of the membrane decreases. Results of the contact angle of synthesized PVDF/TTIP membranes before and after thermal treatment are represented in Table 1. For non-treated membrane the water contact angle of 130±3° obtained where for thermally treated membrane due to enhanced hydrophobicity, the water contact angle increases up to 145±5°. Hydrophobicity enhancement results in an apparent decrease in the permeability of the membranes, in addition, liquid entry pressure (LEP) of the thermally treated membrane is higher than none treated membrane (see Table1). Considering both bad and good aspects of membrane thermal treatment, one compromise must be made between these properties to increase both LEP and permeability of the membranes. Asymmetric post treatment of the synthesized PVDF/TTIP membranes is a promising method for achieving this compromise. For this reason, the produced membrane had both surfaces treated in different manners. The membrane side, which is in contact of the feed stream, must be increased in hydrophobicity to prevent membrane pores wetting by aqueous feed. In contrast, the opposite surface of the membrane must be hydrophilic to enhance the permeate flux. Therefore, thermal treatment of the permeate side surface of the membrane not only improves the membrane performance but also in many cases causes a decrease in membrane permeability. Then, synthesized PVDF/TTIP membranes are just thermally treated in one surface and another side of the membrane is chemically baked using NaOH (0.1 M) solution. For selective thermal treatment of membrane, we used specifically designed stainless steel module for this purpose (see Fig. 2), in which membrane was interposed in contact with two separate chambers. Hot and dry air stream (120 °C) flows through the one surface of the membrane where the other side of membrane is treated in contact with NaOH solution (0.1 M, 50 °C) for 2 hr. After asymmetric post treatment of the membrane for property change study, FT-IR wettability and permeability tests were conducted. FT-IR spectra

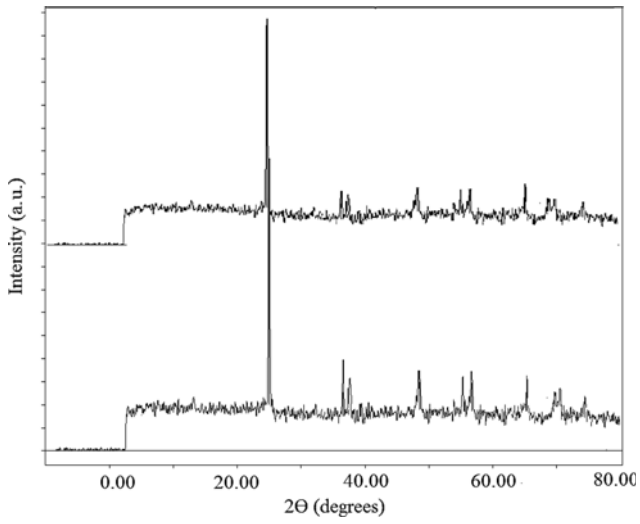


**Fig. 7. XRD patterns of the prepared membrane before thermal treatment M3 (up) and after thermal treatment M'3 (down).**

proved deprotonation in reducing of Ti-OH peak intensity (Fig. 6). In addition, from Fig. 7 XRD crystallographic analyses indicate that the thermally treated PVDF/TTIP membranes contain enhanced crystallization zones compared to non-treated ones.

The thermal treatment causes thickening of the synthesized nanofibers [30]. Furthermore, due to the sol-gel reaction of TTIP particles formed on the nanofibers surface, which causes an increase of surface roughness. The membrane surface roughness can be seen in AFM image of Fig. 8. Sol-gel reaction of TTIP promotes the polycondensation rate with enhancing deprotonation steps. Deprotonation eliminates hydroxyl groups which leads to the improvement of surface hydrophobicity [30].

As mentioned earlier, the surface roughness is one of the main parameter to influence the surface hydrophobicity. AFM analyses were performed for better evaluation of the influence of $TiO_2$ addition on the nanofibers surface roughness. The AFM 3D images and the cross section profiles along the single nanofiber's length direction of PVDF and PVDF/$TiO_2$ nanofibers are depicted in Fig. 8 As shown the PVDF nanofiber (Fig. 8(a)) has a relatively smooth surface in comparison with PVDF/$TiO_2$ hybrid nanofiber. In addition, regarding cross section curves the pristine nanofibers exhibit less irregularity in structure along the direction of length, i.e., the observed irregularity is in the range of 20 nm. On the other hand, the hybrid fibers result in surface irregularity of about 50 nm in the measured cross section curve. This observation confirms that the $TiO_2$ incorporation enhances the surface roughness of nanofibers.

LEP test results show that for the post-treating the surface of the membrane, greater hydrostatic pressure could be applied; this is due to narrower pore size as well as the higher hydrophobicity of this side of the membrane. These exclusive properties of asymmetric post-treated PVDF/TTIP hybrid membrane makes them promising for membrane distillation application. The electrospun PVDF/

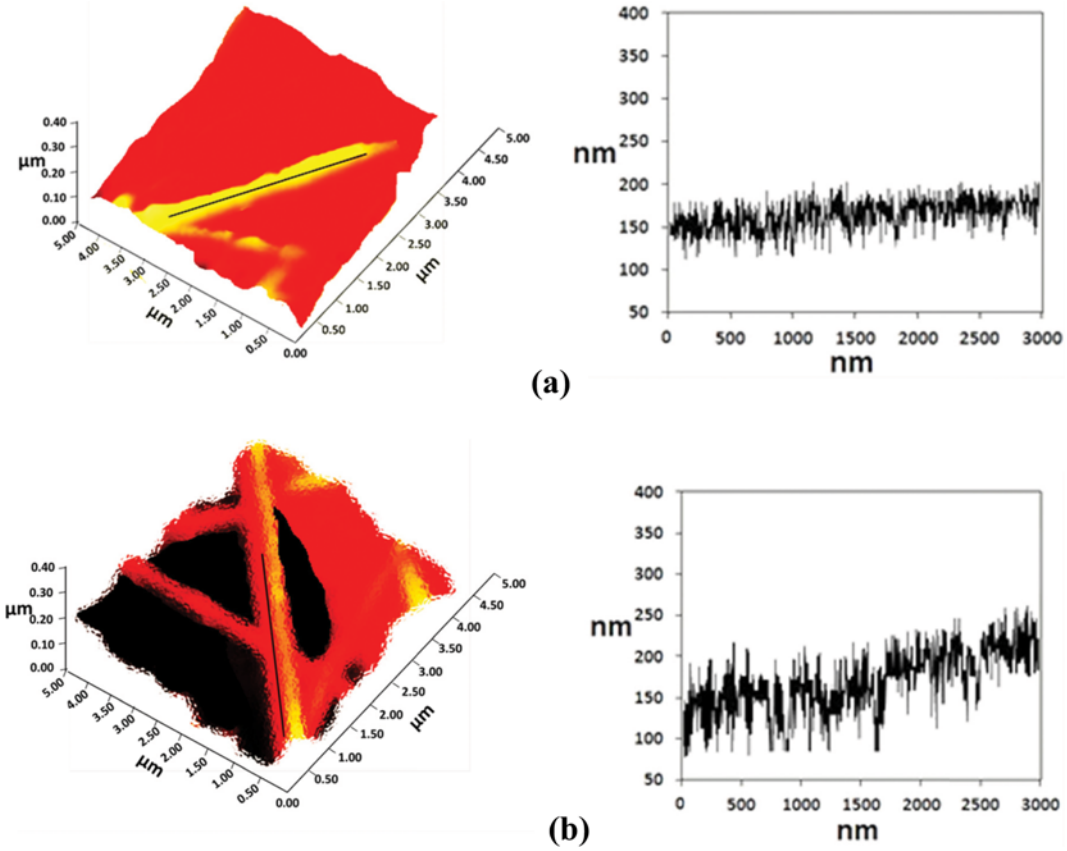


**Fig. 8. AFM images and the roughness analyses along the marked directions (a) PVDF and (b) PVDF/$TiO_2$ nanofiber.**

TTIP hybrid membranes were synthesized and then asymmetric post-treatment was used for trace contaminant removal of heavy metals by vacuum enhanced membrane distillation method.

**2. Pure Water VMD Experiments**

The first step was to obtain optimized values for parameters of feed temperature, flow rate, permeate flux and applied vacuum for the sample synthetic membrane within the new membrane module. For this purpose, pure water VMD was performed with the M1, M3 and M′3 membranes and the results were evaluated to compare different types of synthesized membranes besides identifying of better conditions for the main VMD experiments in the next steps.

The first set of experiments was performed at a constant feed flow rate and permeate applied vacuum of 100 ml/min and 2,500 Pa, respectively. The feed temperature was varied from 40 °C to 80 °C and the VMD pure water permeation flux was measured. The achieved results for three different types of synthesized membranes are shown in Fig. 9. For each PVDF synthetic membrane, with increasing of the feed temperature the permeate flux increases. Pristine PVDF membrane (M1), showed relatively greater permeate flux in comparison with PVDF-TTIP hybrid membrane, but for the feed rate higher than 500 ml/min in many cases membrane departure occurred. Asymmetric post-treated hybrid membranes let to achieve maximum permeate flux at the same feed temperatures compared to other types of membranes. The permeate flux increasing with feed flow rate is because of decreasing in the boundary layer thickness and resistance as well as increasing the Reynolds number (Re) [32]. Achieved results for permeate fluxes in various feed rate show that asymmetric post-treated PVDF-$TiO_2$ membranes in comparison with two other types M1 and M3 have higher permeate flux; on the other hand for low feed rates, pristine nanofibrous PVDF membrane (M1) permeate fluxes are in the range of 5-8 kg/$m^2$ h, which is comparable with M3 and M′3 permeate fluxes. Permeate flux of non-treated and symmetric treated membranes are less than asymmetric treated membranes. This is due to dual hydrophobic/hydrophilic properties of two different sides of the asymmetric thermally post-treated membranes.

For investigating the effect of feed temperature in the permeate flux of pure water through the synthesized membrane pores, a series of VMD tests were carried out in the different temperatures of the hot feed at fixed flow rate and permeate pressure. Fig. 9 illustrates the permeate flux changes versus the feed temperature. It is obvious that with increasing in the feed temperature the permeate flux increases in the result of a higher temperature gradient across the membrane. Also, it could be mentioned that permeate flux is directly proportional to feed flow rate and temperature. At higher temperatures (>80 °C) the permeation process is interrupted due to the turbulence of the feed stream as well as the departure in the membrane structure. The optimized temperature for the VMD tests was 60 °C, considering the better compromise between permeate flux and energy consumed for the heating of the feed stream up to the desired temperature. The permeate flux for the M1, M3 and M3′ membranes is represented in Fig. 9. The obtained results for the permeate flux show that at the same feed temperature M′ membrane likely exhibits greater permeation values, wherein for the pristine PVDF membranes these values are not comparable with other two types at low temperatures.

The effects of applied vacuum of permeate side pressure ($P_p$) of the module during VMD tests on the membrane flux have been studied and the achieved results are depicted in Fig. 10. Applying the vacuum stimulates the permeate flux in the VMD processes due to increasing the vapor pressure difference across the membrane pores. For M1 virgin membranes, the change in permeate pressure strongly affects the permeate flux but for the hybrid membrane, this increase is less sharp. Nevertheless, there is a breakthrough in the applied vacuum in the $P_p$=500 Pa. For pressures less than this value, the pore-wetting phenomenon occurs in all type of membranes. Precise studies show that there is a little differ-

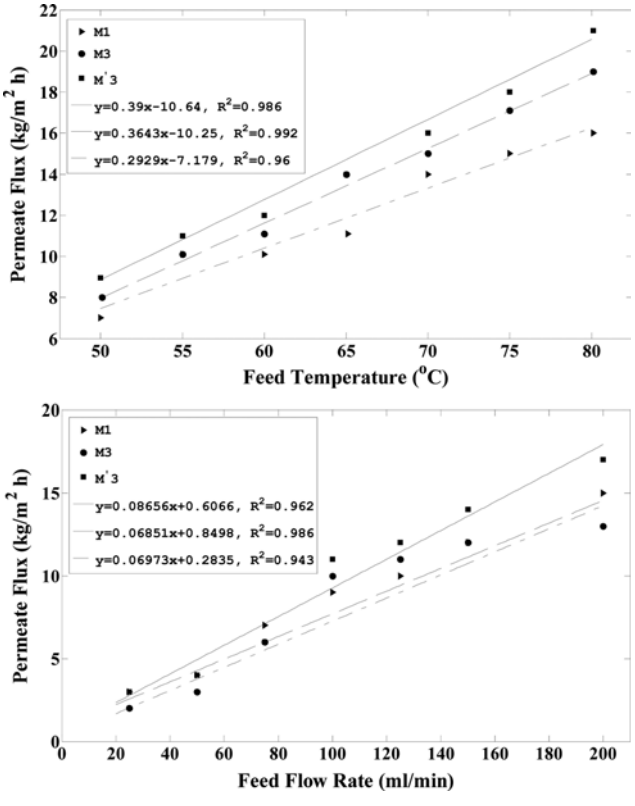


**Fig. 9. Effect of feed flow rate and feed temperature on permeate flux.**

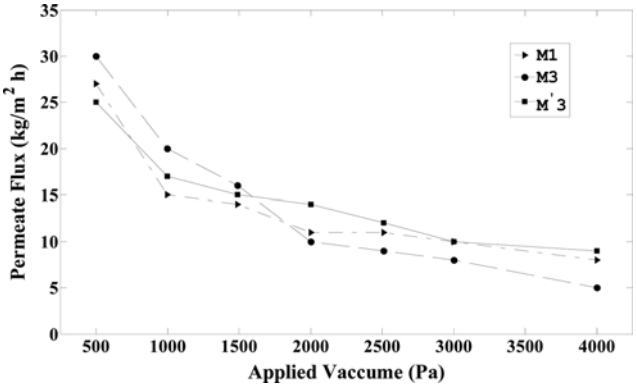


**Fig. 10. Effect of vacuum pressure on the permeate flux.**

ence in the breakthrough permeates pressure for used different types of membranes. In the case of M1, M3, and M'3 membranes $P_p$ values are, respectively, 500, 450 and 600 Pa.

Pure water VMD experiments showed that the optimum process conditions are at higher inlet feed temperatures (65-70 °C), optimized permeate pressure at the range of 2,000-2,500 Pa and feed flow rate of 100 ml/min. Previous studies proved that in this range of temperature, regarding the highest permeate volumes that were obtained, the energy consumption per unit of the permeate product was lower than for lower inlet feed temperatures [32,33].

**3. Contaminated Water VMD Experiments**

There are a few studies in the field of MD use for heavy metal contaminant removal [32-36]. Especially for trace removal of non-volatile heavy metals using MD methods, there is no significant work. In this step, VMD performance was evaluated for total removal of trace metallic contaminants in laboratory scale. Heavy metal trace contaminant removal experiments were carried out by the VMD technique and the same VMD manifold of pure water experiments was used.

The feed solution contains different trace concentrations of various heavy metals [(Co(II), Zn(II), Cu(II), Ni(II), Cd(II), Pb(II)) all in the specific concentration (10-100 ppm)]. Feed stream was heated to 65 °C and then flowed into the module, which the synthesized PVDF-$TiO_2$ hybrid membrane, M′3, was interposed inside it. Water molecules permeate through the membrane pores in the result of vapor pressure difference that are enhanced by applying vacuum in the permeate side of the module. The permeate flux increasing with the vacuum is represented in Fig. 9. In spite of desired permeate flux increasing, greater vacuum causes some side effects, as decreasing in the separation performance and membrane departures. Fig. 10 shows that in the vacuum values greater than 2,000 Pa the membrane pores become wetted in practice and at 1,000 Pa membrane departure takes place. The better compromise between higher permeate flux and unwanted side effects of vacuum is in the range of 2,000-2,500 Pa. In this vacuum, the permeate flux across the membrane is about 10 lit/$m^2$ h; furthermore, trace contaminant removal is obtained in this condition, whereas in the higher vacuums due to the pore wetting of the membranes, the separation efficiency is reduced. LEP tests identify the appropriate pressure difference across the membrane pores. For M3 membrane, this value is higher than other types that allow apply higher vacuums.

VMD experiments with metal salts showed that the ions of the dissolved salts did not pass through the membrane pores and all of them were retained in the retentate. The total concentrations changes of the heavy metal ions in the feed and permeate streams were monitored using metrohm conductivity-meter. Fig. 11 represents the conductivity of the feed or retentate versus running time. The observed increasing in the conductivity of the retentate is due to concentrating of heavy metal ions. The total concentration of the feed solution was changed from 250 ppm to 750 ppm, which caused increasing the conductivity from 120 μS/cm to 600 μS/cm. On the other hand, the conductivity of the distillate stream was almost constant at the same time period. The distillate conductivity gradually decreased by increasing in the permeate volume.

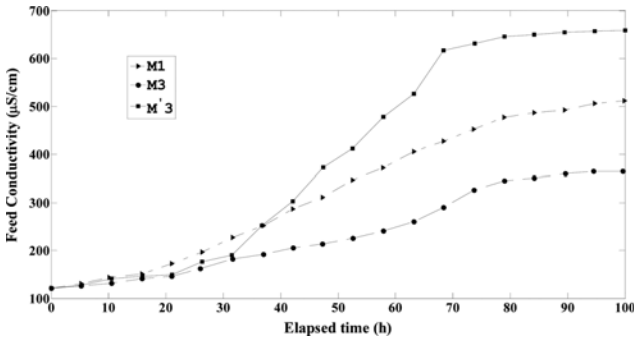


**Fig. 11. Conductivity changes for retentate versus running time.**

For better evaluation of the M′3 asymmetric post-treated PVDF-titania membrane, the same experiments at the similar conditions were carried out using M1 and M3 membranes. The achieved conductivity-metric results are shown in Fig. 11. The concentrating rate of the retentate stream for the M′3 membrane was a little greater than other ones. This is due to greater permeation flux of the asymmetric post-treated PVDF-titania membranes that shown in Fig. 9.

For individually analyzing of each metal ions, we used induced coupled plasma atomic absorption spectroscopy (ICP-AAS) to precisely determine trace concentration. It was observed that the total rejection of heavy metal ions for M′3 and M3 membrane occurred where M1 pristine PVDF membrane could not block the heavy metal leakage into distillate stream through the pores. For investigating of this observation, we analyzed the after used membranes. FT-IR analyses showed that in the case of hybrid PVDF/TTIP non-treated membranes after using the membrane in the MD process a great amount of hydroxyl group formed on the membrane surface as well as inside the pores. The sharp enhancement in the 3,000 $cm^{-1}$ shown in Fig. 6 is due to this hydroxylation process of the membrane nanofibers. These hydroxyl groups could easily adsorb the heavy metal ions, which are diffused into the membrane pores. Considering MD principals, the absorption of metal ions in the membrane matrix during the process could not be beneficial in the long-term running because of fluctuation of the membrane pores [37,38]. This absorption phenomenon is dominant at high concentrations levels of the ion solutes in the feed streams, and for the trace concentrations of the heavy metal ions not only does not affect the separation performance but also could be beneficial in total removal of solutes.

For M′3 asymmetric post-treated PVDF/TTIP membranes hydroxylation did not occur in after used membranes. This is due to the calcination process of the membranes that reduces the potential of forming Ti-O-Ti bonds in the nanofibers structure. As mentioned earlier, wettability, analyses (Fig. 7) indicate that the hydrophobicity of the thermally treated side of PVDF/TTIP membranes was obviously enhanced in comparison with non-treated and pristine membranes. So in comparison with these membrane types, diffusion of aqueous solutes in the M3 membrane pores rarely occurred, which improves the separation performance. In addition, asymmetric thermal-treated M′3 membranes, due to their hydrophobic/hydrophilic dual characteristics, have larger permeate flux, which reduces the running time of the VMD experiments. The permeate conductivity versus the running time for M1, M2, and M′3 synthetic membranes. With increasing in the VMD running time

the metallic ions concentration in the feed streams increases, while after 7 h VMD running the permeate flux decreases for the M1 pristine membranes. Furthermore, the presence of metal ions in the permeated steam was been detected. M2 non-treated hybrid membranes permeate flux began to decrease after 10 hrs passed from experiment running time and this value for the M'3 treated membranes was about 12 hr. Trace contaminant concentration took place in the feed container up to 500% of initiate concentrations when we employed M'3 asymmetric post-treated PVDF/TTIP membranes, without permeation of heavy metal ions into permeate streams or fluctuation of membrane and significant decreasing in permeate flux. But when we used M1 and M3 membranes, although the concentration of solutes at the same level was achieved, but the heavy metal ions leakage into permeate streams occurred because of membrane pore wetting and permeate flux decreasing because of pore fouling taking place in both membrane types.

## CONCLUSION

The performed study confirms that asymmetric post-treated PVDF-$TiO_2$ hybrid membranes could be successfully employed in vacuum enhanced membrane distillation process for total removal of trace heavy metal contaminants and ultra-pure water producing in one step. Improving the VMD drawbacks as low permeate fluxes with introducing of hydrophobic/hydrophilic dual characteristics into the PVDF/TTIP membrane has been examined. VMD experiments demonstrate that this kind of hybrid membrane possesses superior properties in compression with non-treated or virgin membranes.

The introduction of Ti-O-Ti condensed structure into the PVDF electrospun membrane dramatically increased the membrane performance in terms of durability, enrichment enhancement etc., but did not improve the permeate flux of the membrane. With asymmetric thermal treatment of this kind of hybrid membrane, we obtained the results that indicated the increasing in the permeate flux of the membrane without affecting the separation and concentration performance.

## REFERENCES


1. S. Meng, J. Mansouri, Y. Ye and V. Chen, *J. Membr. Sci.*, **450**, 48 (2014).
2. N. Palanisami, K. He and S. Moon, *Korean J. Chem. Eng.*, **31**, 155 (2014).
3. E. Curcio and E. Drioli, *Sep. Purif. Rev.*, **34**, 35 (2005).
4. M. S. El-Bourawi, Z. Ding, R. Ma and M. Khayet, *J. Membr. Sci.*, **285**, 4 (2006).
5. G. L. Liu, C. Zhu, C. S. Cheung and C. W. Leung, *Heat Mass Transf.*, **34**, 329 (1998).
6. S. Yarlagadda,V. G. Gude, L. M. Camacho, S. Pinappu and S. G. Deng, *J. Hazard. Mater.*, **192**, 1388 (2011).
7. W. P. Zhu, S. P. Sun, J. Gao, F. J. Fu and T. S. Chung, *J. Membr. Sci.*, **456**, 117 (2014).
8. M. P. Godino, L. Pena, C. Rincón and J. I. Mengual, *Desalination*, **108**, 91 (1997).
9. A. G. Fane, *Solar heated membrane distillation; energy research and development corporation*, University of New South: Canberra, Australia (1992).
10. P. P. Zolotarev, V. V. Ugrozov, I. B. Volkina and V. M. Nikulin, *J. Hazard. Mater.*, **37**, 77 (1994).
11. X. Wang, L. Zhang, H. Yang and H. Chen, *Desalination*, **247**, 403 (2009).
12. A. Razmjou, E. Arifin, G. Dong, J. Mansouri and V. Chen, *J. Membr. Sci.*, **415-416**, 850 (2012).
13. X. M. Xue and F. T. Li, *Micropor. Mesopor. Mater.*, **116**, 116 (2008).
14. A. Dastbaza and A. R. Keshtkar, *Appl. Surf. Sci.*, **293**, 336 (2014).
15. V. Mottaghitalab and A. Khodaparast Haghi, *Korean J. Chem. Eng.*, **28**(1), 114 (2011).
16. M. Macias, A. Chacko, J. P. Ferraris and K. J. Balkus, *Micropor. Mesopor. Mater.*, **86**, 1 (2005).
17. C. L. Shao, H. Y. Kim, J. Gong, B. Ding, D. R. Lee and S. J. Park, *Mater. Lett.*, **57**, 1579 (2003).
18. A. Bottino, G. Capannelli, V. D'Asti and P. Piaggio, *Sep. Purif. Technol.*, **22**, 269 (2001).
19. J. H. Li, Y. Y. Xu, L. P. Zhu, J. H. Wang and C. H. Du, *J. Membr. Sci.*, **326**, 659 (2009).
20. T. Ogoshi and Y. Chujo, *J. Polym. Sci. A: Polym. Chem.*, **43**, 3543 (2005).
21. L. Y. Yu, Z. L. Xu, H. M. Shen and H. Yang, *J. Membr. Sci.*, **337**, 257 (2009).
22. L. Y. Yu, Z. L. Xu, H. M. Shen and H. Yang, *J. Membr. Sci.*, **337**, 257 (2009).
23. K. Smolders and A. C. M. Franken, *Desalination*, **72**, 249 (1989).
24. M. Khayet, C. Y. Feng, K. C. Khulbe and T. Matsuura, *Polymer*, **43**, 3879 (2002).
25. M. C. Garcıa-Payo, M. Essalhi and M. Khayet, *J. Membr. Sci.*, **347**, 209 (2010).
26. J. K. Young, H. A. Chang and M. O. Choi, *European Polym. J.*, **46**, 1957 (2010).
27. X. Zhang, Y. Wang, Y. You, H. Meng, J. Zhang and X. Xu, *Appl. Surf. Sci.*, **263**, 660 (2012).
28. S. S. Choi, Y. S. Lee, C. W. Joo, S. G. Lee, J. K. Park and K. S. Han, *Electrochim. Acta*, **50**, 339 (2004).
29. A. VenkateswaraRao, H. M. Sakhare, A. K. Tamhankar, M. L. Shinde, D. B. Gadave and P. B. Wagh, *Mater. Chem. Phys.*, **60**, 268 (1999).
30. W. L. McCabe, J. C. Smith and P. Harriott, Unit Operations of Chemical Engineering, 4th Ed., Chemical Engineering Series, McGraw-Hill, New York (1985).
31. G. Zakrzewska-Trznadel M. Harasimowicz and A. G. Chmielewski, *J. Membr. Sci.*, **163**, 257 (1999).
32. J. Blanco Gálvez, L. García-Rodríguezb and I. Martín-Mateosc, *Desalination*, **246**, 567 (2009).
33. G. Zakrzewska-Trznadel, *Nukleonika*, **51**, 101 (2006).
34. G. Zakrzewska-Trznadel and M. Harasimowicz, *Desalination*, **162**, 191 (2004).
35. G. Zakrzewska-Trznadel, M. Harasimowicz and A. G. Chmielewski, *Sep. Purif. Technol.*, **23**, 617 (2001).
36. M. S. El-Bourawi, Z. Ding, R. Ma and M. Khayet, *J. Membr. Sci.*, **285**, 4 (2006).
37. M. Gryta, *Sep. Purif. Technol.*, **80**, 293 (2011).